

A general and robust strategy for the synthesis of nearly monodisperse colloidal nanocrystals

Xinchang Pang, Lei Zhao, Wei Han, Xukai Xin and Zhiqun Lin*

Colloidal nanocrystals exhibit a wide range of size- and shape-dependent properties and have found application in myriad fields, including optics, electronics, mechanics, drug delivery and catalysis, to name but a few^{1–3}. Synthetic protocols that enable the simple and convenient production of colloidal nanocrystals with controlled size, shape and composition are therefore of key general importance^{4,5}. Current strategies include organic solution-phase synthesis⁶, thermolysis of organometallic precursors^{4,7}, sol-gel processes⁵, hydrothermal reactions⁸ and biomimetic and dendrimer templating^{9–11}. Often, however, these procedures require stringent experimental conditions, are difficult to generalize, or necessitate tedious multistep reactions and purification. Recently, linear amphiphilic block co-polymer micelles have been used as templates to synthesize functional nanocrystals^{12,13}, but the thermodynamic instability of these micelles limits the scope of this approach. Here, we report a general strategy for crafting a large variety of functional nanocrystals with precisely controlled dimensions, compositions and architectures by using star-like block co-polymers as nanoreactors. This new class of co-polymers forms unimolecular micelles that are structurally stable, therefore overcoming the intrinsic instability of linear block co-polymer micelles. Our approach enables the facile synthesis of organic solvent- and water-soluble nearly monodisperse nanocrystals with desired composition and architecture, including core-shell and hollow nanostructures. We demonstrate the generality of our approach by describing, as examples, the synthesis of various sizes and architectures of metallic, ferroelectric, magnetic, semiconductor and luminescent colloidal nanocrystals.

Owing to their ability to direct the aggregation of inorganic materials in well-defined, confined volumes, micelles of linear amphiphilic block co-polymers offer an attractive means by which to synthesize colloidal nanocrystals, as recently exploited in conjunction with sol-gel chemistry¹⁴. However, conventional linear polymeric micelles are thermodynamic aggregates of amphiphilic molecules above their critical micelle concentration^{14–16}. They are therefore ‘dynamically’ stable, so their characteristics for a given system depend heavily on temperature and solvent properties, and the shape of the micelles may change when experimental conditions, such as concentration, solvent, temperature and pH¹⁷, are varied. Only the nanoparticles that do not require high-temperature conversion from precursors can be prepared in solution by reducing the precursor entrapped within the block co-polymer micelles¹⁴.

In contrast, our method is based on a series of multi-arm star-like block co-polymers comprising either all hydrophilic or hydrophilic/hydrophobic blocks that are covalently linked to a small core. These co-polymers form thermodynamically stable unimolecular micelles (micelles composed of a single co-polymer), the size and shape of which can be tuned by chemical synthesis, and act as nanoreactors for the synthesis of inorganic materials^{17,18}.

The star-like block co-polymers used here are poly(acrylic acid)-block-polystyrene (PAA-*b*-PS) and poly(acrylic acid)-block-poly(ethylene oxide) (PAA-*b*-PEO) diblock co-polymers, and poly(4-vinylpyridine)-block-poly(tert-butyl acrylate)-block-polystyrene (P4VP-*b*-PtBA-*b*-PS), poly(4-vinylpyridine)-block-poly(tert-butyl acrylate)-block-poly(ethylene oxide) (P4VP-*b*-PtBA-*b*-PEO), polystyrene-block-poly(acrylic acid)-block-polystyrene (PS-*b*-PAA-*b*-PS) and polystyrene-block-poly(acrylic acid)-block-poly(ethylene oxide) (PS-*b*-PAA-*b*-PEO) triblock co-polymers. We first synthesized plain nanoparticles using amphiphilic star-like PAA-*b*-PS diblock co-polymer as a template to demonstrate the effectiveness of our strategy for producing a wide spectrum of high-quality nanoparticles (Fig. 1a, Supplementary Table S1, Section SI). The inner PAA block in the unimolecular micelles is hydrophilic and imparts the preferential incorporation of precursors into the interior space occupied by 21 PAA blocks via a strong coordination bonding between the metal moiety of the precursors and the functional groups of PAA (–COOH)¹⁹. It is important to note that there was no such coordination with the outer hydrophobic PS blocks. Subsequent hydrolysis and condensation of appropriate precursors in the mixed solvents of dimethylformamide (DMF) and benzyl alcohol formed the desired nanoparticles with the PAA blocks encapsulated inside (see Supplementary Section SIII for the proposed formation mechanisms), while the surface of the nanoparticles was intimately and permanently connected with hydrophobic PS blocks (Fig. 1a).

The synthesis of ferroelectric PbTiO₃ nanoparticles with different diameters (Fig. 2a) was used as an example to illustrate the protocol depicted in Fig. 1a. Representative high-resolution transmission electron microscopy (HRTEM) characterization of 9.8 ± 0.4 nm PbTiO₃ nanoparticles demonstrated that they had continuous crystalline lattices (Fig. 2a, lower left). The formation of single crystals may be qualitatively understood as follows. The volume fraction of PAA blocks encapsulated in the 9.8 ± 0.4 nm nanoparticle was only ~13.8%, based on thermogravimetric analysis (TGA) measurements (Supplementary Section SIV). Because the reaction temperature was lower than the degradation temperature of the polymer templates ($T_d = 210$ °C according to TGA), the chain segments of the PAA-*b*-PS (for example, AA units) may either substitute the atoms on a specific crystalline lattice of nanoparticles and become part of the lattice structure or may intercalate the lattices, thereby resulting in single crystalline nanoparticles, regardless of the presence of PAA chains. Similar phenomena have been broadly observed in organic molecule/inorganic crystal systems^{20–22}. This will be the subject of future studies.

Intuitively, the volume ratio of DMF to benzyl alcohol in the mixed solvents had a profound influence on the shape uniformity of the resulting nanoparticles. Indeed, tailoring the solubility of polymer chains using mixed selective solvents can facilitate the encapsulation of inorganic precursors. This led to a better defined spherical space composed of inner hydrophilic PAA blocks, from

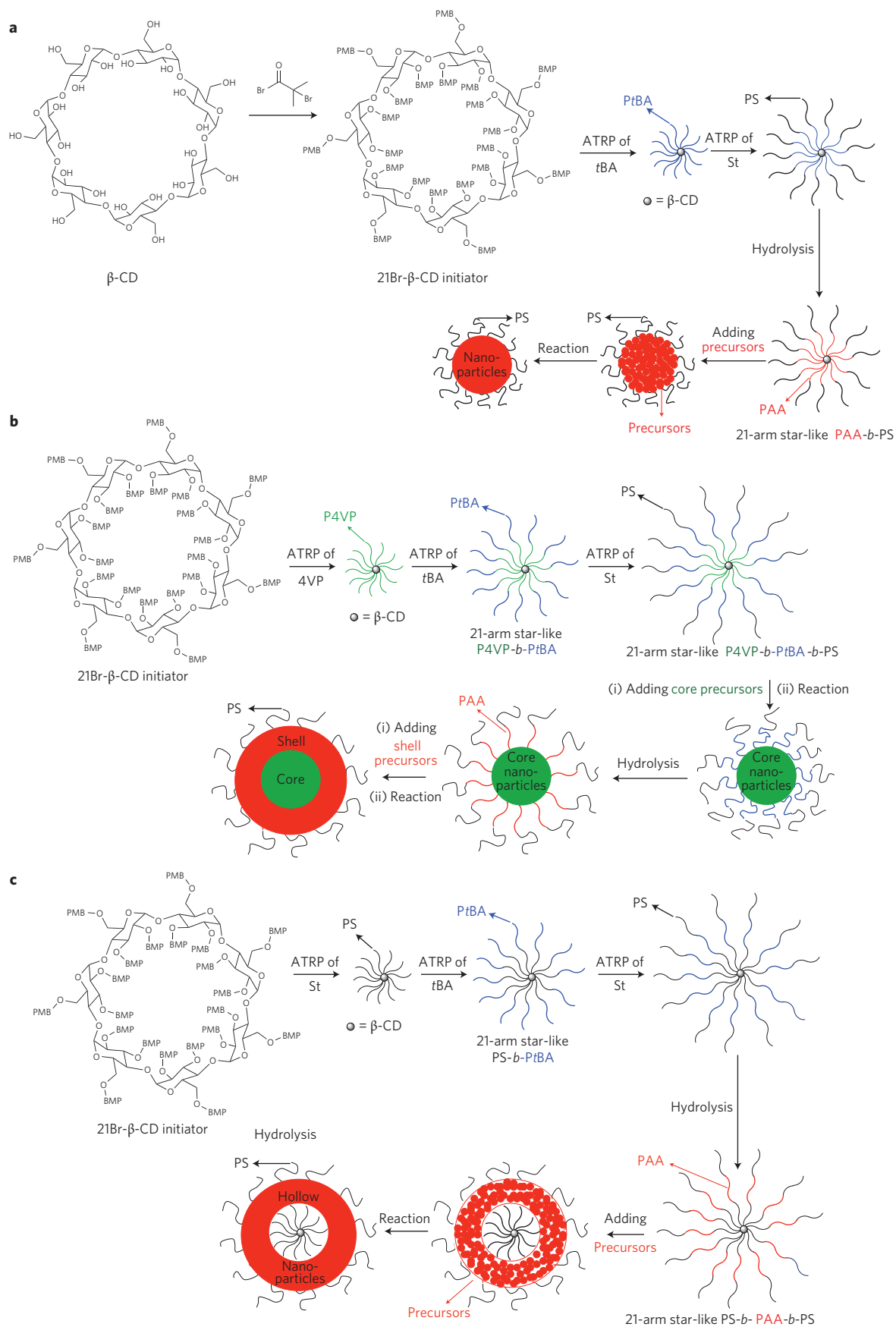


Figure 1 | Schematic representation of synthetic strategies for nanoparticles with different architectures (plain, core-shell and hollow) using amphiphilic star-like block co-polymers as nanoreactors. a–c, Formation of plain nanoparticles (a), core-shell nanoparticles (b) and hollow nanoparticles (c). CD, cyclodextrin; BMP, 2-bromo-2-methylpropanoate; St, styrene.

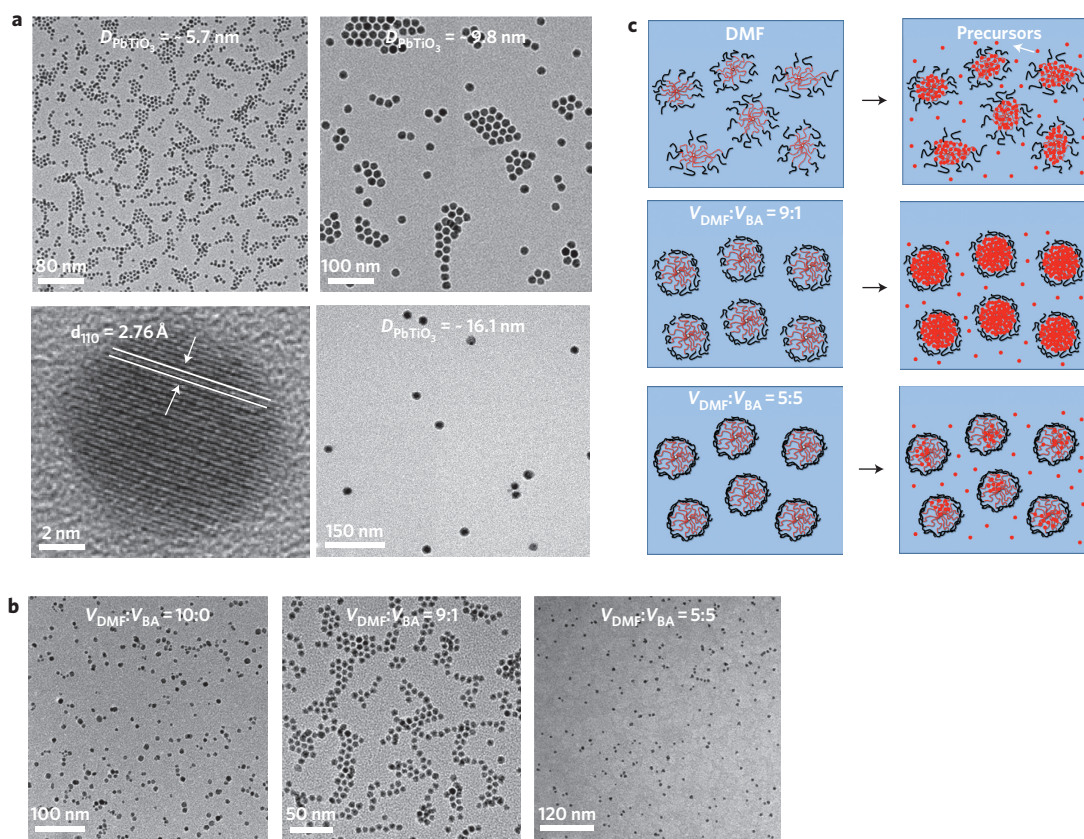


Figure 2 | Formation of plain nanoparticles. **a**, TEM images of three PbTiO_3 nanoparticles with different diameters prepared using three star-like PAA-*b*-PS templates with different molecular weights of PAA block as nanoreactors (see also samples A–C in Supplementary Table S1). An HRTEM image of the 9.8 ± 0.4 nm nanoparticle is shown (lower left), demonstrating a continuous crystalline lattice with a lattice spacing of 2.76 Å, corresponding to the (110) crystalline plane of the tetragonal phase of PbTiO_3 , suggesting the formation of a single-crystal structure. **b**, TEM images of PbTiO_3 nanoparticles (sample A in Supplementary Table S1) formed in a mixture of DMF and benzyl alcohol (BA) at different volume ratios. **c**, Proposed mechanism for the growth of uniform ($V_{\text{DMF}}:V_{\text{BA}} = 9:1$) and non-uniform ($V_{\text{DMF}}:V_{\text{BA}} = 10:1$ and $V_{\text{DMF}}:V_{\text{BA}} = 5:5$) nanoparticles in DMF and benzyl alcohol. The mechanism for the growth of nearly monodisperse nanoparticles can be rationalized by considering the solubility of each block in DMF and benzyl alcohol. The star-like PAA-*b*-PS can be readily dissolved in DMF, forming unimolecular micelles (**c**, upper left). With the addition of benzyl alcohol, a good solvent for PAA but a non-solvent for PS, the outer PS blocks collapse due to unfavourable interaction between PS and benzyl alcohol, while the inner PAA blocks retain a coil-like conformation. At $V_{\text{DMF}}:V_{\text{BA}} = 9:1$, a transition from the expanded chain conformation in pure DMF (**c**, upper left) into a more compact and structurally stable spherical macromolecule occurs (**c**, centre left). The density of inner PAA blocks (that is, the number of chains per volume) increases slightly, resulting in small chain-length shrinkage. This is observed by comparing the TEM image of **a** with the dynamic-light-scattering measurements in Supplementary Table S7. At the same time, the loading of precursors into this well-defined regime composed of PAA chains increases, yielding nanoparticles with markedly improved uniformity (**a** and **b**, centre). However, with the addition of more benzyl alcohol ($V_{\text{DMF}}:V_{\text{BA}} = 5:5$), a significant collapse of the outer PS chains is observed (**c**, lower left), making it difficult for precursors to enter the PAA phase, and thus forming non-uniform nanoparticles (**b**, right).

which nanoparticles nucleate and grow. This mixed solvent approach is key to our method (Fig. 2c). When DMF alone was used as the solvent, PbTiO_3 nanoparticles had relatively irregular shapes (DMF:benzyl alcohol = 10:0 by volume; Fig. 2b, left). With a 9:1 DMF:benzyl alcohol solvent ratio, PbTiO_3 nanoparticles were produced with the best uniformity (Fig. 2b, centre). As more benzyl alcohol was added (DMF:benzyl alcohol = 5:5), the shape regularity of nanoparticles decreased again (Fig. 2b, right). The mechanism for the growth of nanoparticles in the mixed solvents at different volume ratios is illustrated in Fig. 2c.

Surprisingly, the strategy for our star-like block co-polymer nanoreactor for nanoparticle synthesis is quite general. It can be readily extended to produce a large variety of nanoparticles with good uniformity (with most of the size distribution lying within 5% of the average size) and solubility, including noble metal, ferroelectric, magnetic and semiconductor nanoparticles. These different types of nanoparticle are shown in the representative TEM images of Fig. 3 (their crystalline lattices are shown both in the insets to Fig. 3 and in Supplementary Fig. S21) and as digital images in

Supplementary Fig. S22. The possible mechanisms for forming PbTiO_3 , TiO_2 and ZnO nanoparticles are proposed in Supplementary Figs S2–S4. Metallic platinum nanoparticles were also prepared and are shown in Supplementary Fig. S23. Energy-dispersive spectroscopy (EDS) microanalysis and X-ray diffraction (XRD) measurements confirmed the successful synthesis of these materials (Supplementary Section SVIII). These functional nanoparticles are intrinsically linked to outer hydrophobic PS blocks, imparting good solubility in organic solvents (such as toluene, tetrahydrofuran (THF), chloroform, dichloromethane, DMF and so on). Furthermore, the presence of hydrophobic PS blocks is also crucial to ensuring the miscibility of nanoparticles with the host environment, retaining the unique properties of the nanoparticles by preventing them from aggregating.

In many instances it is highly desirable to prepare water-soluble nanoparticles connected with hydrophilic ligands for use in biomedical applications²³. To this end, by changing the template from amphiphilic star-like PAA-*b*-PS to a double-hydrophilic star-like PAA-*b*-PEO diblock co-polymer synthesized by a combination of atom transfer

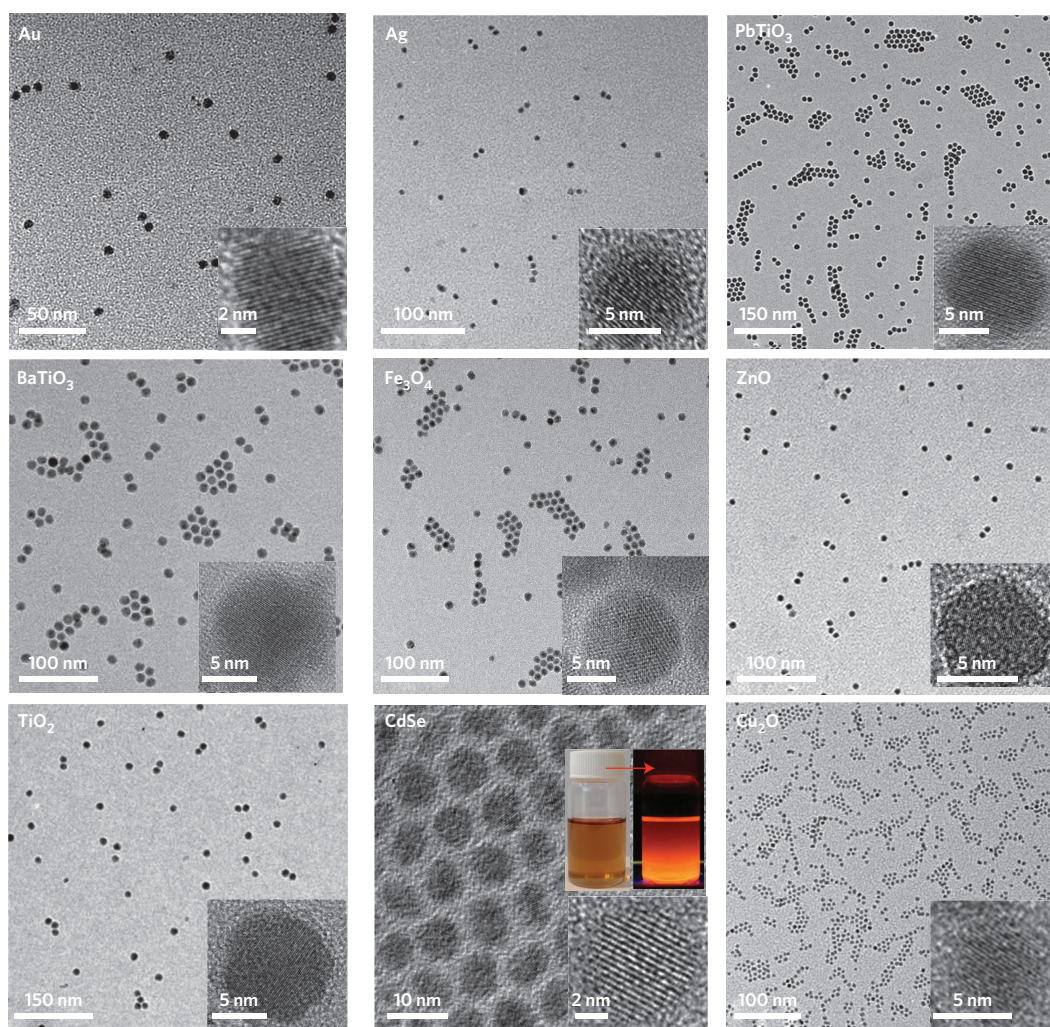


Figure 3 | Representative TEM images of a variety of nanoparticles synthesized using star-like PAA-*b*-PS templates (samples A, B and D in Supplementary Table S1). The images show noble metal (gold, with surface plasmonic properties, Supplementary Fig. S18; silver), ferroelectric (PbTiO₃ and BaTiO₃), magnetic (Fe₃O₄, exhibiting superparamagnetic properties, Supplementary Fig. S19) and semiconductor (n-type ZnO, n-type TiO₂; luminescent CdSe, showing optical properties, Supplementary Fig. S20; p-type Cu₂O) nanoparticles. Diameters of nanoparticles: noble metal ($D_{Au} = 5.8 \pm 0.2$ nm, $D_{Ag} = 6.1 \pm 0.3$ nm); ferroelectric ($D_{PbTiO_3} = 9.7 \pm 0.4$ nm, $D_{BaTiO_3} = 10.4 \pm 0.3$ nm); magnetic ($D_{Fe_3O_4} = 10.1 \pm 0.5$ nm); and semiconductor ($D_{ZnO} = 6.3 \pm 0.3$ nm, $D_{TiO_2} = 10.2 \pm 0.2$ nm, $D_{CdSe} = 6.2 \pm 0.3$ nm, $D_{Cu_2O} = 6.4 \pm 0.2$ nm). Insets: the crystalline lattices of each nanoparticle are clearly evident in HRTEM images. Corresponding digital images of the nanoparticles are shown in Supplementary Fig. S22. Digital images of CdSe nanoparticles before (left) and after (right, emitting red fluorescence) ultraviolet illumination are shown as insets (bottom, centre).

radical polymerization (ATRP) and click reaction (Supplementary Section SI-1), a series of water-soluble plain nanoparticles (for example, gold, Supplementary Fig. S26; platinum, Supplementary Fig. S27; and Fe₃O₄, Supplementary Fig. S28) were also produced successfully (Supplementary Scheme S1, Table S2, Section SVII).

Of particular interest is the fact that our strategy for producing highly crystalline nanoparticles is remarkably versatile. In addition to plain nanoparticles, we also synthesized core-shell nanoparticles. Core-shell nanostructures are conventionally obtained by dissimilar materials epitaxy, which requires moderate lattice mismatches (<2%) between the two different materials so as to obtain the high-quality core-shell heterostructures that would otherwise be difficult to achieve^{24,25}.

As outlined in Fig. 1b, our general strategy for using a new class of star-like triblock co-polymers as nanoreactors enables the creation of a wide range of core-shell nanoparticles with well-controlled size of the core and shell materials, as well as different compositions and properties. Possible nanoparticle combinations include, but are not limited to, metal-semiconductor or

semiconductor-metal, metal-metal oxide or metal oxide-metal, and dissimilar metal oxide core-shell nanoparticles, as verified by XRD measurements (Supplementary Figs S49, S51–S53).

Similarly, the growth of core-shell nanoparticles was based on the coordination reaction between functional blocks in the star-like triblock co-polymer and the respective precursors (Fig. 1b). The size of the core and shell materials can be readily tuned by altering the length of the first P4VP block and the second P*t*BA block (hydrolysed into PAA later), respectively. More importantly, because the growth of the shell is completely templated by the functional second block of the triblock co-polymer, the shell lattice structure can be independent of the core material²⁴, thus circumventing the limitations imposed with epitaxial growth.

We chose the synthesis of core-shell magnetic-ferroelectric Fe₃O₄-PbTiO₃ nanoparticles as an example. The Fe₃O₄ core (Fig. 4a, left) was first formed by the encapsulation of its precursors within the innermost P4VP regime through a selective coordination interaction between the nitrogen atoms of the P4VP blocks (Fig. 1b) and the metal moieties of the precursors (see the proposed

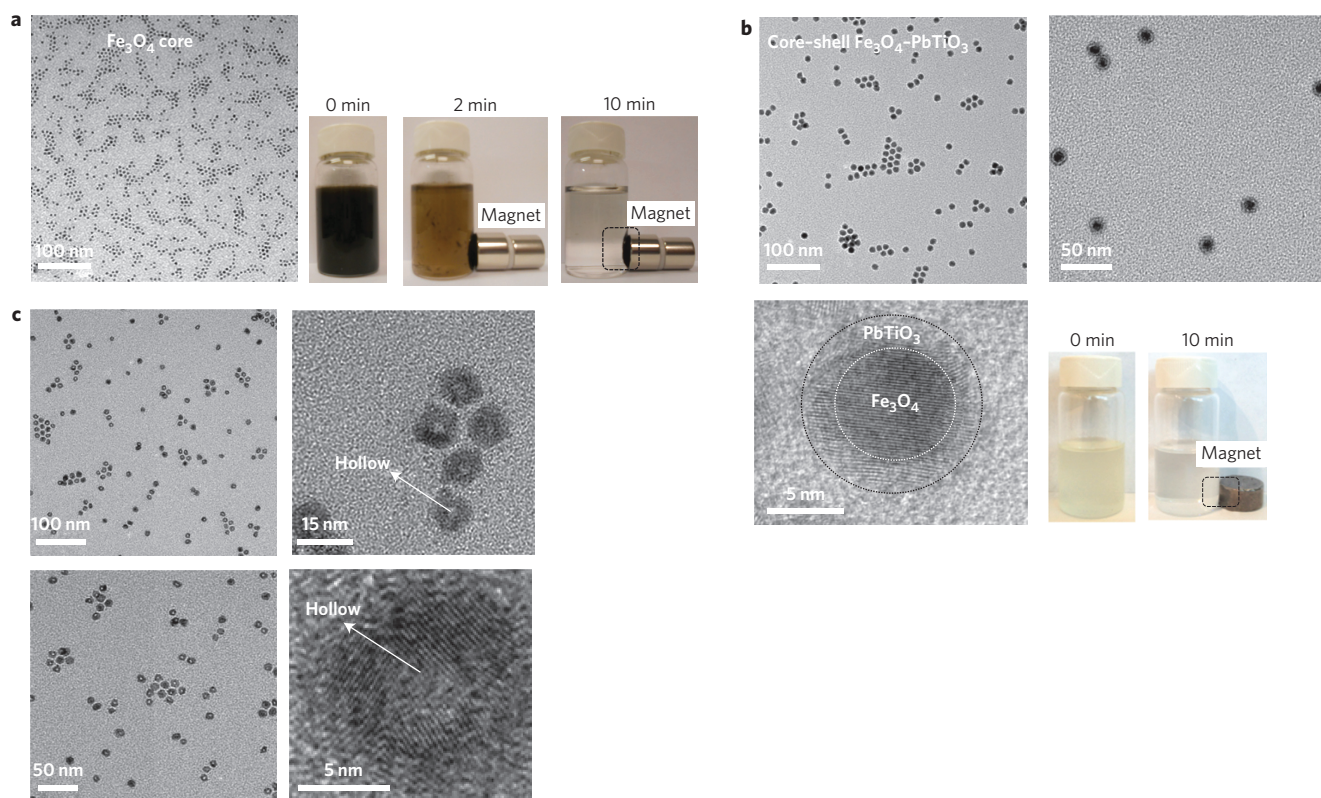


Figure 4 | TEM and digital images of Fe_3O_4 - PbTiO_3 core-shell nanoparticles and TEM images of hollow gold nanoparticles formed using star-like triblock co-polymers as nanoreactors. **a,b, TEM images of Fe_3O_4 core (**a**, $D_{\text{Fe}_3\text{O}_4} = 6.1 \pm 0.3$ nm) and Fe_3O_4 - PbTiO_3 core-shell nanoparticles at different magnifications (**b**, PbTiO_3 shell thickness = 3.1 ± 0.3 nm). Fe_3O_4 appears dark. An HRTEM image (lower left panel, **b**) clearly shows the crystalline lattices of the Fe_3O_4 core and PbTiO_3 shell (white and black dashed circles for guidance). The magnetic properties of the Fe_3O_4 - PbTiO_3 nanoparticles were retained, as clearly shown in the digital images of a nanoparticle toluene solution, which show the nanoparticles deposited on the wall of the vials under the influence of magnetic bars (marked with black boxes) (**a**, central, $t = 2$ min; right, $t = 10$ min). For Fe_3O_4 core materials only, the toluene solution appears dark at high concentrations, resulting from the Fe_3O_4 (**a**, left, $t = 0$ min). For Fe_3O_4 - PbTiO_3 core-shell nanoparticles, the toluene solution appears white, resulting from the PbTiO_3 shell (**b**, left, $t = 0$ min). **c**, TEM images of representative hollow gold nanoparticles with a uniform size distribution (thickness of gold, 3.2 ± 0.3 nm; diameter of hollow core, 5.6 ± 0.4 nm).**

formation mechanism in Supplementary Fig. S5)¹⁴. Subsequently, the PtBA blocks situated on the surface of the Fe_3O_4 core were thermally hydrolysed into PAA (Supplementary Section SIII). The PbTiO_3 shell was then formed by using the PAA blocks as a template (Supplementary Fig. S6). Figure 4b presents TEM images of Fe_3O_4 - PbTiO_3 nanoparticles (Fig. 4b, upper panels) with uniform size and narrow size distribution. The crystalline PbTiO_3 shell is clearly evident in the HRTEM image in Fig. 4b (lower left; 3.1 ± 0.3 nm thick). The crystal structures of Fe_3O_4 and PbTiO_3 were further corroborated by XRD and EDS measurements (Supplementary Figs S52, S67). Strikingly, despite more than 40% lattice mismatch between Fe_3O_4 and PbTiO_3 (ref. 24), the Fe_3O_4 - PbTiO_3 nanoparticles were successfully synthesized using our star-like triblock co-polymer template strategy. Similarly, other core-shell nanoparticles can also be produced as long as appropriate precursors are identified (for example, Fe_3O_4 -Au in Supplementary Figs S5, S7, S29, and Au-CdSe in Supplementary Fig. S30).

In addition to organic solvent-soluble core-shell nanoparticles, water-soluble core-shell nanoparticles can also be produced. Using a triple-hydrophilic star-like P4VP-*b*-PAA-*b*-PEO triblock co-polymer (Supplementary Section SI-2) as the nanoreactor, water-soluble core-shell nanoparticles (for example, Fe_3O_4 -Au, Supplementary Fig. S31; base metal-noble metal Sn-Pt, Supplementary Fig. S32), intimately connected with hydrophilic PEO blocks, were created (Supplementary Scheme S2, Table S4, Section SVII).

Interestingly, amphiphilic star-like triblock co-polymers can also be used to structure-direct precursors into hollow, nearly monodisperse nanoparticles by selectively sequestering precursors in the intermediate block and growing into nanoparticles. Hollow noble-metal nanoparticles are the subject of intense research for use in bioimaging, photothermal therapy and drug delivery²⁶. We prepared hollow gold nanoparticles using our star-like PS-*b*-PAA-*b*-PS triblock co-polymer template (Supplementary Table S5, Section SI-3). The gold precursors were confined in the intermediate PAA regime (Fig. 1c), and ultimately yielded hollow gold nanoparticles with hydrophobic PS blocks intimately tethered on both the inside and outside of the gold surface. Notably, members of this intriguing class of nanoparticles may be regarded as organic-inorganic core-shell nanoparticles (for example, with a PS core and a gold shell).

It is not surprising that TEM characterization clearly demonstrated that the gold nanoparticles were morphologically hollow, appearing bright in their centre (Fig. 4c). The highly crystalline nature of the hollow nanoparticles is apparent in the HRTEM image, where the crystalline lattice partially appears in the centre. This can be attributed to the presence of the crystalline gold shell above and below the hollow core. Moreover, the composition and elemental distribution of hollow structures mapped by EDS and XRD measurements further proved the successful formation of hollow gold nanoparticles (for example, Supplementary Fig. S56). The size of such hollow nanoparticles can be conveniently

controlled by varying the length of the innermost PS block and intermediate PtBA block during ATRP, thus allowing for the production of a variety of hollow nanoparticles with different sizes, including hollow semiconductor Cu₂O nanoparticles (Supplementary Fig. S33). Similarly, water-soluble hollow nanoparticles (for example, gold, Supplementary Figs S34, S57) linked with hydrophilic PEO blocks can also be produced using star-like PS-*b*-PAA-*b*-PEO triblock co-polymer as the nanoreactor (Supplementary Scheme S3, Table S6, Section SVII).

The unimolecular micelle-template strategy we have described enables the synthesis of nearly monodisperse nanoparticles with precisely controllable size and surface chemistry, and including plain, core-shell and hollow nanostructures. The permanent connection between the nanoparticles and the respective hydrophobic or hydrophilic polymer chains renders them soluble in either organic or aqueous environments, respectively. Our approach can be readily extended to nearly all the transition or main-group metal ions and organometallic ions. We envisage that more complex nanoparticles with multifunctional shells (for example, core-shell 1-shell 2, core-shell 1-shell 2-shell 3) may also be made using star-like tetra-block and pentablock co-polymer templates, with the possibility of crafting desired arbitrary nanostructures for fundamental studies in nanoscience. Finally, in addition to inorganic colloidal nanocrystals, the method we have reported may also be viable for the synthesis of polymeric nanoparticles by selectively crosslinking intermediate blocks of star-like block co-polymers, suggesting potential applications as nanocapsules for the release of drugs, inks and so on^{1,26}.

Methods

Synthesis of nanoparticles using star-like block co-polymers as nanoreactors. For plain nanoparticles, 10 mg star-like PAA-*b*-PS template was dissolved in a 10 ml mixture of DMF and benzyl alcohol at room temperature ($V_{\text{DMF}}:V_{\text{BA}} = 9:1$), followed by the addition of appropriate amounts of precursors (for example, PbTi[OCH(CH₃)₂]₆) that were selectively incorporated into the inner PAA blocks. The molar ratio of acrylic acid (AA) units in the PAA block to precursor was set at 1:5 to maximize the loading of precursors into the PAA domains. The mixture was then refluxed at elevated temperature for a period of time (for example, 180 °C for 2 h for PbTiO₃). For core-shell nanoparticles, 10 mg star-like P4VP-*b*-PtBA-*b*-PS template was dissolved in a 10 ml mixture of DMF and benzyl alcohol at room temperature ($V_{\text{DMF}}:V_{\text{BA}} = 9:1$). The core material was first formed by the encapsulation of its precursors (for example, FeCl₂·4H₂O:FeCl₃·6H₂O:ammonium hydroxide = 1:1:1 by mole for Fe₃O₄) within the innermost P4VP regime, followed by reaction at a certain temperature for a period of time (for example, 50 °C for 30 min for Fe₃O₄). Similarly, the molar ratio of the 4-vinylpyridine (4VP) unit of the P4VP block to precursors was 1:5. Subsequently, the PtBA blocks were hydrolysed into PAA by annealing in phenyl ether at 200 °C for 2 h. The shell materials were then formed by carrying out the reaction (for example, refluxing at 180 °C for 2 h for PbTiO₃ using PbTi[OCH(CH₃)₂]₆ as precursor) with the use of PAA blocks as template while keeping the other experimental conditions the same. For hollow nanoparticles, 10 mg star-like PS-*b*-PAA-*b*-PS template was dissolved in a 10 ml mixture of DMF and benzyl alcohol at room temperature ($V_{\text{DMF}}:V_{\text{BA}} = 9:1$). Similarly, the precursor (for example, HAuCl₄) and reducer (such as ethanol, if applicable) were subsequently added into the template solution. After the reaction (for example, at 60 °C for 10 h for gold), hollow nanoparticles (for example, gold) with PS blocks tethered on both the inside and outside were obtained (see Supplementary Section SVII for experimental details). For the synthesis of water-soluble nanoparticles (plain, core-shell and hollow) linked with hydrophilic PEO blocks, see Supplementary Section SVII.

Synthesis of nanoparticles using linear block co-polymers as templates. To compare the use of star-like block co-polymers with linear block co-polymer counterparts as nanoreactors for the synthesis of nanoparticles under the same experimental conditions, linear block co-polymers (PAA-*b*-PS, P4VP-*b*-PtBA-*b*-PS and PS-*b*-PAA-*b*-PS) with similar molecular weights and ratios of the different blocks to those of star-like block co-polymers were also synthesized by ATRP. Instead of nanoparticles like those produced using star-like block co-polymer templates, large irregular aggregates were formed when the corresponding linear block co-polymers were used as templates in the mixture of DMF and benzyl alcohol ($V_{\text{DMF}}:V_{\text{BA}} = 9:1$). A detailed comparison (a mechanistic study) is presented in Supplementary Section SX.

Received 10 December 2012; accepted 12 April 2013;
published online 2 June 2013

References

- Langer, R. Drug delivery and targeting. *Nature* **392**, 5–10 (1998).
- Wang, X., Zhuang, J., Peng, Q. & Li, Y. A general strategy for nanocrystal synthesis. *Nature* **437**, 121–124 (2005).
- Sun, S., Murray, C. B., Weller, D., Folks, L. & Moser, A. Monodisperse FePt nanoparticles and ferromagnetic FePt nanocrystal superlattices. *Science* **287**, 1989–1992 (2000).
- Peng, X. G. *et al.* Shape control of CdSe nanocrystals. *Nature* **404**, 59–61 (2000).
- Yang, P., Zhao, D., Margolese, D. I., Chmelka, B. F. & Stucky, G. D. Generalized syntheses of large-pore mesoporous metal oxides with semicrystalline frameworks. *Nature* **396**, 152–155 (1998).
- Murray, C. B., Norris, D. J. & Bawendi, M. G. Synthesis and characterization of nearly monodisperse CdE (E = sulfur, selenium, tellurium) semiconductor nanocrystallites. *J. Am. Chem. Soc.* **115**, 8706–8715 (1993).
- Park, J. *et al.* Ultra-large-scale syntheses of monodisperse nanocrystals. *Nature Mater.* **3**, 891–895 (2004).
- Liang, Y. *et al.* Co₃O₄ nanocrystals on graphene as a synergistic catalyst for oxygen reduction reaction. *Nature Mater.* **10**, 780–786 (2011).
- Chiu, C. *et al.* Platinum nanocrystals selectively shaped using facet-specific peptide sequences. *Nature Chem.* **3**, 393–399 (2011).
- Crooks, R. M., Zhao, M., Sun, L., Chechik, V. & Yeung, L. K. Dendrimer-encapsulated metal nanoparticles: synthesis, characterization, and applications to catalysis. *Acc. Chem. Res.* **34**, 181–190 (2000).
- Juttukonda, V. *et al.* Facile synthesis of tin oxide nanoparticles stabilized by dendritic polymers. *J. Am. Chem. Soc.* **128**, 420–421 (2005).
- Chai, J., Wang, D., Fan, X. & Buriak, J. M. Assembly of aligned linear metallic patterns on silicon. *Nature Nanotech.* **2**, 500–506 (2007).
- Nie, Z., Petukhova, A. & Kumacheva, E. Properties and emerging applications of self-assembled structures made from inorganic nanoparticles. *Nature Nanotech.* **5**, 15–25 (2010).
- Leong, W. L. *et al.* Non-volatile organic memory applications enabled by *in situ* synthesis of gold nanoparticles in a self-assembled block copolymer. *Adv. Mater.* **20**, 2325–2331 (2008).
- Riess, G. Micellization of block copolymers. *Prog. Polym. Sci.* **28**, 1107–1170 (2003).
- Darling, S. B. Directing the self-assembly of block copolymers. *Prog. Polym. Sci.* **32**, 1152–1204 (2007).
- Pang, X., Zhao, L., Akinc, M., Kim, J. K. & Lin, Z. Novel amphiphilic multi-arm, star-like block copolymers as unimolecular micelles. *Macromolecules* **44**, 3746–3752 (2011).
- Newkome, G. R., Moorefield, C. N., Baker, G. R., Saunders, M. J. & Grossman, S. H. Unimolecular micelles. *Angew. Chem. Int. Ed.* **30**, 1178–1180 (1991).
- Kidambi, S., Dai, J., Li, J. & Bruening, M. L. Selective hydrogenation by Pd nanoparticles embedded in polyelectrolyte multilayers. *J. Am. Chem. Soc.* **126**, 2658–2659 (2004).
- Kahr, B. & Gurney, R. W. Dyeing crystals. *Chem. Rev.* **101**, 893–952 (2001).
- Rohl, A. L., Gay, D. H., Davey, R. J. & Catlow, C. R. A. Interactions at the organic/inorganic interface: molecular modeling of the interaction between diphosphonates and the surfaces of barite crystals. *J. Am. Chem. Soc.* **118**, 642–648 (1996).
- Bullard, T. *et al.* Role of kinks in dyeing crystals: confocal luminescence microscopy from single molecules to square centimeters. *Cryst. Growth Des.* **9**, 982–990 (2009).
- Medintz, I. L., Uyeda, H. T., Goldman, E. R. & Mattoussi, H. Quantum dot bioconjugates for imaging, labelling and sensing. *Nature Mater.* **4**, 435–446 (2005).
- Zhang, J., Tang, Y., Lee, K. & Ouyang, M. Nonepitaxial growth of hybrid core-shell nanostructures with large lattice mismatches. *Science* **327**, 1634–1638 (2010).
- Palmstrom, C. J. Epitaxy of dissimilar materials. *Annu. Rev. Mater. Sci.* **25**, 389–415 (1995).
- Im, S. H., Jeong, U. & Xia, Y. Polymer hollow particles with controllable holes in their surfaces. *Nature Mater.* **4**, 671–675 (2005).

Acknowledgements

The authors acknowledge funding support from the Air Force Office of Scientific Research (FA9550-09-1-0388 and FA9550-13-1-0101) and the Georgia Institute of Technology. The authors also thank Y. Xia and V. Tsukruk for helpful discussions.

Author contributions

Z.L. and X.P. conceived and designed the experiments. X.P., L.Z., W.H. and X.X. performed the experiments. Z.L., X.P., L.Z., W.H. and X.X. analysed the data. Z.L., X.P. and L.Z. wrote the paper. All authors discussed the results and commented on the manuscript.

Additional information

Supplementary information is available in the [online version](#) of the paper. Reprints and permissions information is available online at www.nature.com/reprints. Correspondence and requests for materials should be addressed to Z.L.

Competing financial interests

The authors declare no competing financial interests.